

Paris Basin VSPs: case history establishing combinations of fine-layer (or lithologic) anisotropy and crack anisotropy from modelling shear wavefields near point singularities

Iain Bush* and Stuart Crampin

British Geological Survey, Murchison House, West Mains Road, Edinburgh, EH9 3LA, UK

Accepted 1991 July 26. Received 1991 July 5; in original form 1991 April 9

SUMMARY

This paper examines shear-wave splitting in multi-offset VSPs at a borehole site in the Paris Basin, and demonstrates that the sedimentary structure must have, at least, orthorhombic anisotropic symmetry. It is suggested that the most likely cause for such an orthorhombic symmetry is the combination of fine-layer (or lithologic) anisotropy and crack anisotropy. Transition zones (close to shear-wave singularities), where there are rapid changes of shear-wave polarizations and delays, can account for the anomalous observed waveforms. Observations of large variations in shear-wave polarizations in propagation directions close to point singularities, are probably the first positive identification of the effects of singularities in sedimentary basins.

Key words: crack (EDA) and fine-layer (PTL) anisotropy, sedimentary basins, shear-wave singularities, shear-wave splitting.

1 INTRODUCTION

In recent years, shear-wave anisotropy has increasingly been used as a tool for investigating, at least the uppermost half, of the Earth's crust. There are many possible applications of shear-wave anisotropy (Crampin 1987a), but its greatest impact will probably be on reservoir characterization. It is estimated that, with the current oil recovery methods, 70 to 80 per cent of mobile oil is left behind after initial extraction-implying a vast resource base of unrecovered oil. Seismology is probably the single most important geophysical technique for investigating inaccessible rock. What is needed, to exploit these data, is a clearer understanding of the relationship between reservoir properties and the internal structure of the rockmass (Nur 1989). Shear-wave anisotropy offers the possibility for monitoring this internal structure for the characterization of hydrocarbon reservoirs (Crampin 1990a).

Anisotropy with respect to wave propagation occurs if a solid has a structural orientation on a scale small compared to the wavelength, which persists over distances that are large compared to the wavelength. The most diagnostic effect on seismic waves is shear-wave splitting, where shear waves split into two components with different velocities and

different polarizations, which are fixed for the particular propagation direction through the anisotropic rock. We shall refer to the faster arrival as $qS1$, and the slower as $qS2$ (Crampin 1989). There appear to be two basic types of anisotropic symmetry in sedimentary basins as follows.

(1) Transverse isotropy (TI) with a vertical axis of symmetry, leading to azimuthal isotropy (Crampin 1989). This can be caused by two phenomena: the horizontal alignment of flattened grains, particularly in shales (Kaarsberg 1968), leading to what we shall call lithologic anisotropy; and the effective anisotropy of finely layered horizontal isotropic strata (see many papers by Levin and Helbig and their colleagues). Both types of TI lead to similar patterns of velocity variations, and since repeated sequences of fine layers lead to convenient analytical formulae for the elastic constants (Postma 1955; Backus 1962), we shall use these formulae to model both types of TI. For convenience, we shall refer to such anisotropy with a vertical symmetry axis as PTL anisotropy (Periodic Thin-Layer anisotropy).

(2) The other characteristic type of anisotropic symmetry in most rocks, including those in sedimentary basins, is the azimuthal anisotropy of approximately vertical fluid-filled inclusions known as extensive-dilatancy anisotropy or EDA (Crampin 1984; Crampin, Evans & Atkinson 1984). This leads to TI with a horizontal axis of symmetry. Formulations for the effective elastic constants of distributions of dry and

* Formerly at: Department of Geology and Geophysics, University of Edinburgh, James Clerk Maxwell Building, Edinburgh, EH9 3JZ, UK. Now at: Geophysikalisches Institut, Universität Fridericiana Karlsruhe, Hertzstrasse 16, Karlsruhe-West (21), D-7500, Germany.

fluid-filled cracks of given aspect ratios have been derived by Hudson (1980, 1981, 1986, 1991) and further developed by Crampin (1984).

This paper demonstrates that combinations of PTL and EDA anisotropy are required to model synthetic seismograms in the multi-offset vertical seismic profiles (VSPs) in the Paris Basin (Crampin & Bush 1986; Bush & Crampin 1987). The main tool of our analysis is matching observations with fullwave synthetic seismograms, by trial and error techniques. The problem is determining initial parameters to begin the search procedure. The main parameters to be estimated are 3-D patterns of polarizations of the faster shear wave and the time separations (time delays) between the split shear waves. We extract this information from the 3-D shear wavefields by analysing polarization diagrams (or hodograms). Polarization diagrams for nearly vertically propagating shear waves are horizontal cross-sections of the particle motion displayed for selected time windows around the initial shear-wave arrival (Crampin 1978).

Techniques for analysing and interpreting shear-wave splitting are being currently developed, which were not available at the time of this study. Use of such techniques would not necessarily change our interpretations, but enable results to be obtained with less effort. In any case, we suggest that polarization diagrams will always be important for studying and verification of anomalous features of shear-wave propagation. The procedure in this study was to examine, and reject, alternative explanations for the shear-wave behaviour, and present the preferred modelling through a combination of PTL and EDA anisotropy. The theoretical behaviour of shear-wave splitting in seismic anisotropy has been investigated by Crampin (1981), and the notation for anisotropy used in this paper is that proposed by Crampin (1989).

2 GEOLOGY

The Paris Basin has been studied extensively by petroleum geologists such as Pages (1987). The 2315 m deep vertical borehole penetrates horizontally bedded sedimentary limestone and shale formations ranging from upper Cretaceous (90 Myr) to lower Jurassic (190 Myr). Well logs of the lithology, sonic velocities, V_p/V_s ratios, and density of the surrounding rockmass, are shown in Fig. 1. The strata under investigation are structurally undeformed and within 2° of horizontal.

In situ stress measurements in the thick limestone layers of the Paris Basin yield a homogeneous stress field NNW-SSE (Froidevaux, Paquin & Souriau 1980), similar to that found elsewhere in central and NW Europe associated with the Alpine orogeny.

3 DATA ACQUISITION

There are several advantages in recording shear waves subsurface in three-component VSPs. It avoids the complicated interactions of shear waves with the free surface (Booth & Crampin 1985), particularly in the presence of low-velocity surface layers, topographic irregularities, and the expected near-surface stress and crack anomalies

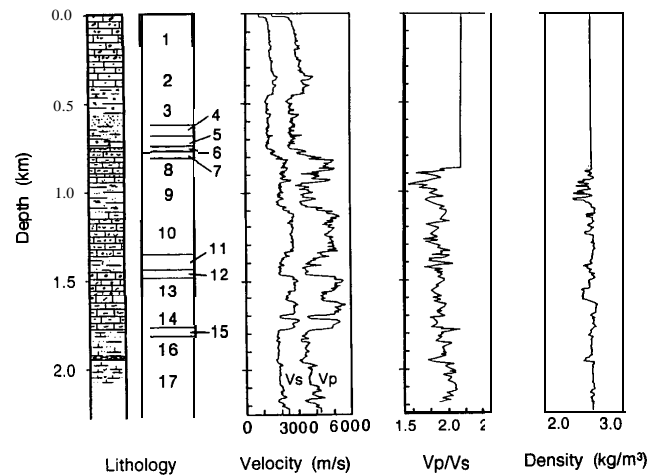


Figure 1. Borehole measurements of lithology; P-wave and shear-wave sonic velocities V_p/V_s log; and density log. Note that only P-wave logs are available above 900 m. Shear-wave velocities above 900 m are determined from P-wave logs assuming that $V_p/V_s = 2.15$. The borehole traverses the following limestone/shale sequence: (1) Ceno-Turonian; (2) Cenomanian; (3) Albian; (4) Aptian; (5) Barremian; (6) Neocomian; (7) Purbeckian; (8) Portlandian; (9) Kimmeridgian; (10) Lusitanian; (11) Oxfordian; (12) Calovian; (13) Bathonian; (14) Bajocian; (15) Aalenian; (16) Toarcian; (17) Pliensbachian.

(Crampin 1990b). In addition, the location of geophones in a borehole, in the zone of interest, allows a more detailed analysis of the reservoir rock than may be achieved with surface geophones (Yardley & Crampin 1991). The three-component VSP survey of a Paris Basin borehole was recorded, in December 1983, by a French VSP Consortium with a series of offset P-wave and shear-wave sources. The positions of the shear-wave source offsets relative to the wellhead and the shear-wave source orientations, are shown in Fig. 2 with details provided in Table 1.

The shear-wave source consisted of two synchronized horizontal vibrators, aligned transverse to the source/borehole direction, except for the near-offset source, SO, which was oriented 53° from radial. The vibrators generated a 10 s linear sweep from 7 to 80 Hz. The depths surveyed in the borehole ranged from 1100 to 2060 m with geophones every 15 m. The recording tool had geophone elements arranged in an orthogonal xyz configuration, with

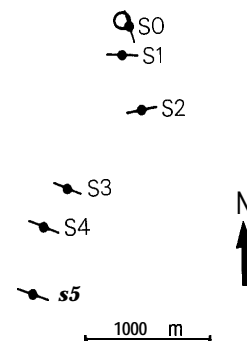


Figure 2. Plan of shear-wave source offsets SO to S5 (solid circles), and source orientations (bars), relative to wellhead (open circle).

Table 1. Details of shear-wave source locations and orientations.

| Offset name | Offset from wellhead (m) | Azimuth from wellhead (N°E) | Vibrator orientation (N°E) |
|-------------|--------------------------|-----------------------------|----------------------------|
| S0 | 68 | 125 | 162 |
| S1 | 272 | 180 | 271 |
| S2 | 727 | 168 | 259 |
| S3 | 1443 | 198 | 290 |
| S4 | 1772 | 199 | 290 |
| S5 | 2311 | 196 | 287 |

a sampling rate of 2 ms. The main modal resonances of the three-component tool are well outside the frequency range of the recorded shear waves and would have negligible effect on the recorded signal (A. Green, private communication).

4 PRE-PROCESSING

The field traces were demultiplexed and sweep cross-correlated, before reorienting the three-component motion.

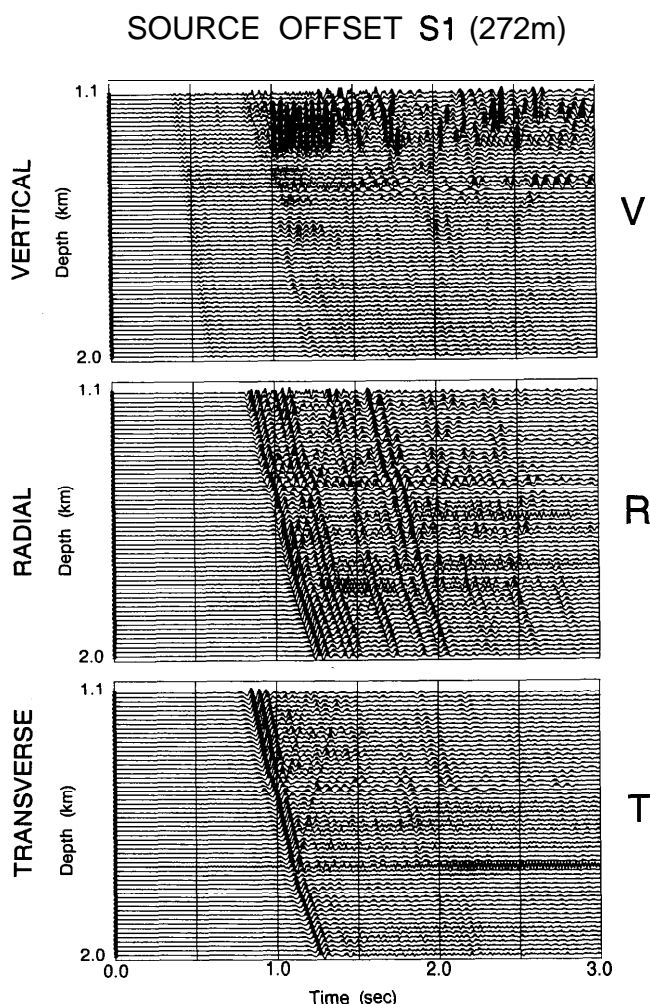


Figure 3. Observed three-component seismicograms for the S1 source offset at an offset of 272 m rotated into Vertical, Radial and Transverse components. Each component (V, R, and T) is individually scaled so relative amplitudes on each component cannot be compared. The relative amplitudes between successive geophone depths are equivalent.

The orientation of the horizontal geophone elements were determined from maximizing the amplitude of the horizontal P-wave displacements, which can be assumed to be parallel to the direction of wave propagation, even in the presence of significant anisotropy (Crampin, Stephen & McGonigle 1982). The presence of 50 Hz electrical interference on the recorded seismicograms (Neville 1986) was found to distort the observed shear-wave motions, and the application of a 0-50 Hz bandpass filter (after rotation) removed the interfering signal without significant change to the shear wavefield. Without further processing, the seismicograms clearly indicate the direct shear-waves arrivals. Fig. 3 shows typical three-component seismicograms for the S1 source location.

5 ANALYSIS OF SHEAR-WAVE SPLITTING

The VSPs were recorded with geophones every 15 m between depths of 1160 and 2060 m for six offsets, S0 to S5, with one offset, S4, repeated. With the exception of offset S5, the polarization diagrams, in general, vary smoothly with depth, and Fig. 4 shows selected diagrams at every 180 m. We shall base our analysis on these selected polarization diagrams. The diagrams displayed little or no continuity at the widest offset, S5, and we suggest this is caused by, possibly quite minor, interface irregularities, whose effects would be less pronounced for ray paths at steeper angles of incidence at the smaller offsets. Less than 10 per cent of the diagrams showed anomalous patterns. Even at levels where the geophone orientations were very different, the repeated offsets S4A and S4B show strong similarities, when rotated into geographical axes as in Fig. 4. This suggests that in general the coupling of the geophones is good, geophone levels are repeatable, and that the polarization patterns represent the true ground motion.

5.1 Estimation of crack orientation

The polarization diagrams in Fig. 4 show systematic behaviour quite unlike what would be expected for propagation through a plane-layered isotropic structure. However, because the time delays are small and the Vibroseis source does not produce an impulsive arrival, classic patterns of shear-wave splitting, where two split shear waves with different polarizations have abrupt onsets (Crampin 1978, 1985a), are only visible at the near zero (68m) offset S0. (We did not attempt to convert to a minimum phase signal, as our experience indicates that shear-wave splitting is difficult to identify in polarization diagrams of minimum phase signals.)

Figure 5 shows detailed diagrams of the three geophones near the top and near the bottom for the S0 offset. Because of the small time delay and emergent onset, the initial shear-wave polarization is visible only for a small segment of the initial shear-wave arrival in a direction approximately N25°W marked by the $qS1$ arrowhead, where $qS1$ is the faster split shear wave. (We shall eventually show that these small segments of the zero-offset profile are the only displacements parallel to the strike of the EDA cracks in all the multi-offset profiles.) The particle motions for this offset have initial displacements ($qS1$ -wave polarizations) generally in the NW/SE direction which suggests shear-wave

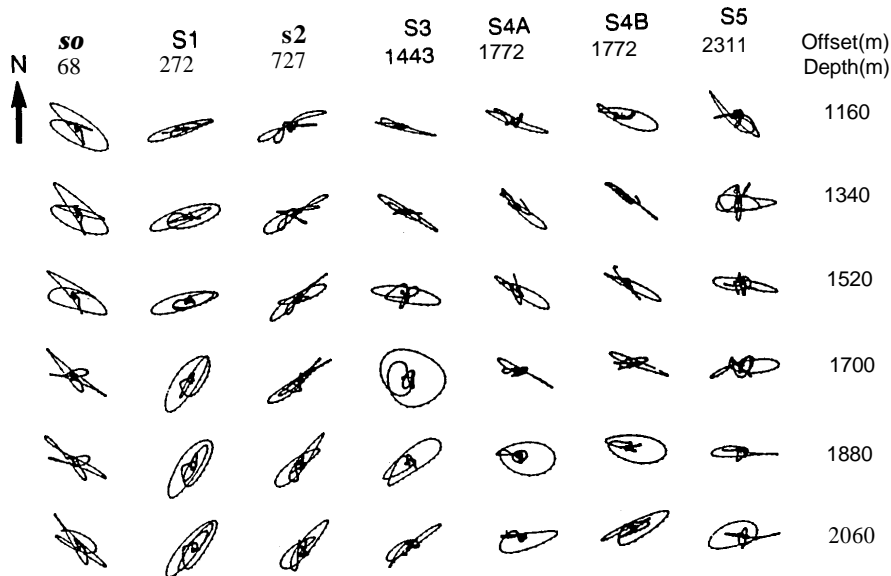


Figure 4. Selection of horizontal polarization diagrams (rotated into geographic coordinates) for a 200 ms time window about the shear-wave arrivals. Six sampling depths are shown for each of seven source positions (including the repeated S4A and S4B offset).

propagation through vertical cracks striking in these quadrants (Crampin 1985a). Supporting this qualitative interpretation, the direction of the compressional stress in the Paris Basin is also believed to be in these quadrants

(Froidevaux et al. 1980), and would be expected to align the cracks (Crampin & Atkinson 1985). The shear waves recorded from the wider source-offsets do not show such distinctive first-motions. This is believed to be due to the smaller time delay between the shear waves in these directions.

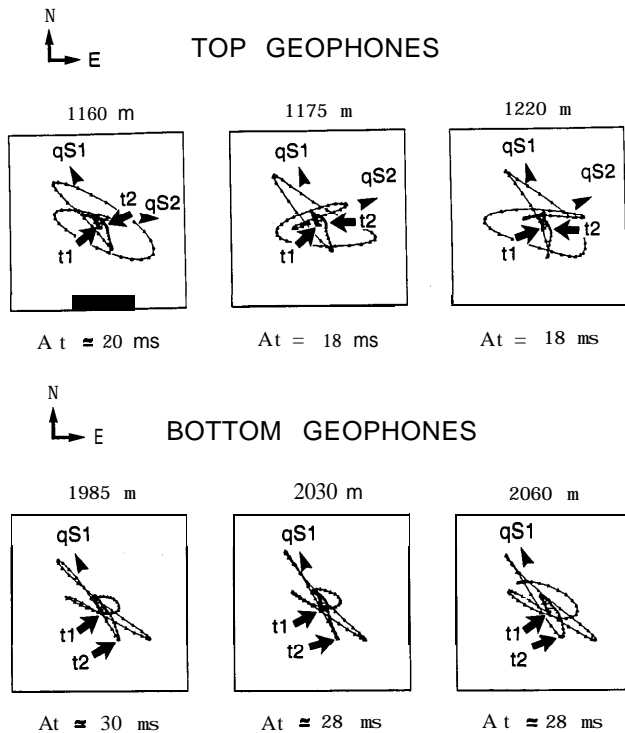


Figure 5. Polarization diagrams of horizontal shear-wave particle motions, recorded at three geophone depths near the top and near the bottom of SO (68 m offset). Arrowheads indicate the interpreted faster (*qS1*-) and slower (*qS2*-wave) polarizations. The *qS2*-wave polarizations are difficult to identify for the bottom geophones since the onsets are emergent. The shear-wave time delays ($A t = t_2 - t_1$) are measured by counting samples between the points marked with arrows: the first arrival t_1 , and an abrupt change in polarization, t_2 .

5.2 Estimation of crack density from shear-wave delays

At the uppermost geophones of the zero-offset profile, SO, the time delay split shear waves is typically 20 ms. Down the geophone column, the nature of splitting changes, as displayed in polarization diagrams, indicating an overall increase in delay, to approximately 28 ms. The increase in shear-wave delays between 1100 and 2000 m is less than that between the surface and 1100 m, suggesting stronger anisotropy near the surface.

From the measured shear-wave traveltimes and delays in the SO profile, we estimate a mean differential shear-wave anisotropy (Crampin 1989) of 2.7 ± 0.2 per cent (from 0 to 1100 m) and 1.8 ± 0.4 per cent (from 1100 to 2060 m). The most likely cause for this anisotropy, along near-vertical travel paths, is the effective anisotropy of vertically aligned EDA cracks (Crampin 1985b). Assuming that the observed shear-wave splitting seen at SO is entirely due to vertically aligned fluid-filled cracks, our estimated shear-wave anisotropies may be converted using the Hudson (1980, 1981) formulations to an approximate crack density (concentration of cracks per unit volume) (Bush 1990). Note that these are mean crack densities and that crack densities may vary with depth. These qualitative results are summarized in Table 2.

6 INITIAL SYNTHETIC MODELLING

The general principle we have adopted, in order to invert the observations of shear-wave splitting, has been to first model the observations at shallow depths, and then

Table 2. Summary of analysis of polarization diagrams from the zero-offset VSP, SO, and interpreted crack properties. Crack density is $N a^3 v$, where N is the number of cracks of radius a in volume v . Errors in the estimated crack densities are derived from the uncertainties in measuring time delays.

| Depth range (m) | Travel time (ms) | Time delay (ms) | Diff. shear-wave anisotropy (%) | Estimated crack density | Estimated crack strike (N°W) |
|-----------------|------------------|-----------------|---------------------------------|-------------------------|------------------------------|
| 0-1100 | 715 ±2 | 20 ±2 | 2.7 f0.2 | 0.024 ±0.004 | 25 ±10 |
| 1100-2060 | 1159 ±2 | 28 ±2 | 1.8 f0.2 | 0.016 ±0.005 | 25 ±10 |

successively work down the geophone column modifying the model parameters appropriately. In applying this layer-stripping approach, we have only considered horizontally layered models of the Earth, and have subjectively minimized the misfit between observed and synthetic seismograms. We define the optimal model as: (1) producing synthetic seismograms which are the best subjective match of the observed records; (2) containing the minimum complications (requiring the least number of parameters); and (3) being most physically plausible.

We have used the computer package of Taylor (1987, 1990) to calculate synthetic seismograms by an extension of the anisotropic reflectivity technique (Booth & Crampin 1983). Since no information about the emitted wavelet at the source was available, we have calculated synthetic seismograms for a wavelet best matching the observed shear-wave motions recorded at the geophones. As the source pulse is probably modified significantly by the near-surface layering (Yardley & Crampin 1991), this procedure might well be necessary even if the source pulse were available.

6.1 Isotropic background model

In order to establish a structure in which to insert cracks, we initially considered an isotropic background model of two horizontal layers over a half-space, with velocities and densities representative of the sonic logs. The parameters of this model are given in Table 3. Ray paths for this model and comparison with the well logs are shown in Fig. 6.

The shear-wave arrival times for this isotropic structure (not shown) agree well with the observed times, and synthetic and observed polarization diagrams for this model are shown in Fig. 7. The linear, or nearly linear, synthetic patterns of displacement in the diagrams are not similar to the sometimes complicated observed patterns. Clearly, a plane layered isotropic model does not model the observed polarization diagrams.

Table 3. Average three-layered isotropic velocity model (interpreted from sonic logs).

| Layer thickness (m) | Depth to top of layer (m) | Density ρ (kg/m ³) | P-wave velocity (m/s) | S-wave velocity (m/s) |
|---------------------|---------------------------|-------------------------------------|-----------------------|-----------------------|
| 800 | 0 | 2600 | 2800 | 1300 |
| 1000 | 800 | 2600 | 4350 | 2350 |
| halfspace | 1800 | 2600 | 3600 | 1800 |

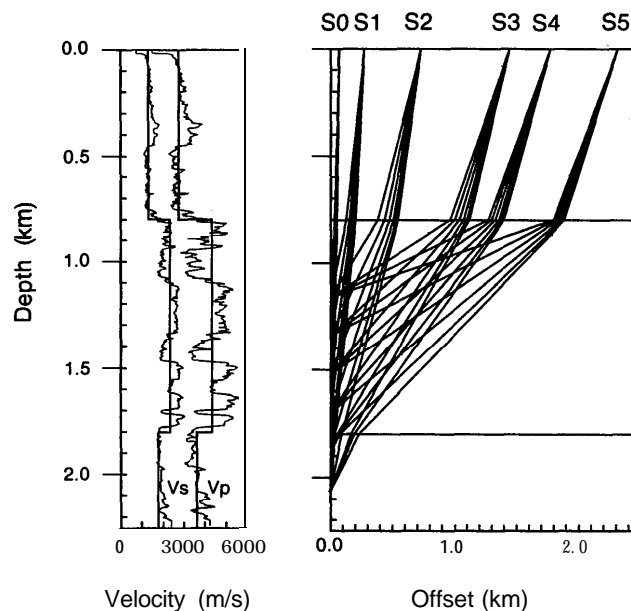


Figure 6. P-wave and shear-wave velocities and ray paths for three-layered isotropic model with parameters in Table 3.

6.2 Finely layered model

The sonic velocities in Fig. 1 fluctuate over vertical intervals of a few metres, suggesting evidence for fine layering with thicknesses less than the seismic wavelength (PTL anisotropy) in the vicinity of the borehole. The very fine variations are interpreted as individual fractures in the well bore (no televiewers or dipmeter logs were available). Shear-wave propagation through the finely layered model (not shown), representative of the sonic log fluctuations, reveals linear particle motion at all source offsets similar to those in Fig. 7. Such linear particle motion is expected, since all vertical planes are symmetry planes so that the shear waves are polarized either qSV or qSH .

6.3 Model with lithologic anisotropy

The presence of shale in the Paris Basin (Fig. 1) may also contribute to the anisotropy due to the effects of aligned grains. Horizontally bedded shale is azimuthally isotropic, that is transversely isotropic with a vertical symmetry axis (Kaarsberg 1968). Consequently, for the same reasons as fine-layer anisotropy discussed previously, shale would not account for the observed shear-wave splitting along near-vertical ray paths.

6.4 Model containing vertically aligned crack inclusions

Using the crack formulations of Hudson (1980, 1981) and Crampin (1984), we define a model of vertically aligned fluid-filled cracks of negligible aspect ratio, with crack densities interpreted from the data in Table 2. Synthetic polarization diagrams calculated for a range of crack orientations in the NW/SE quadrants, indicate that the greatest similarity between observed and synthetic diagrams for the zero-offset profile, SO, is when cracks are aligned between N30°W and N45°W (Bush 1990). This alignment of

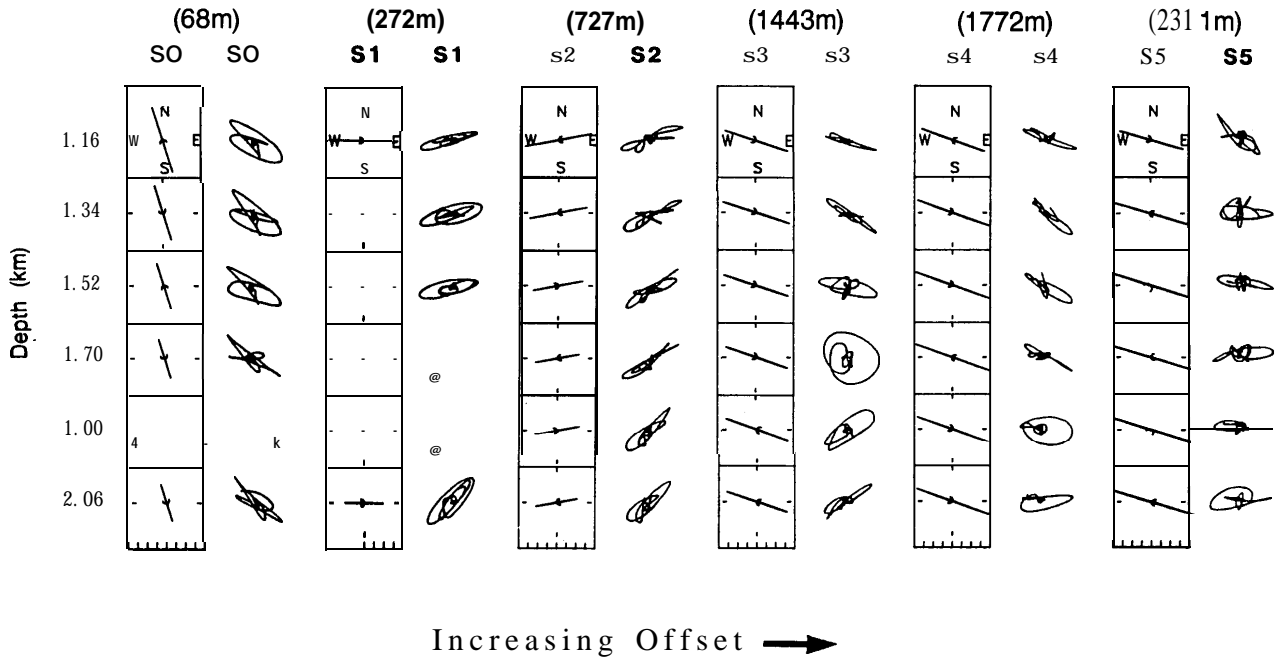


Figure 7. Observed shear-wave polarization diagrams (open columns) compared with synthetic diagrams (boxed columns) from the three-layered isotropic model.

cracks broadly agrees with our previous interpretation obtained from the shear-wave polarizations in the polarization diagrams of the SO offset. Synthetic diagrams calculated for a narrower range of crack orientations indicate that different crack orientations match better particular offsets, but synthetic seismograms for cracks

oriented N30°W provide a reasonable match for all the observed polarization diagrams.

Figure 8 shows polarization diagrams for the model described in Table 4. We suggest that the match of synthetic to observed patterns in the diagrams is a good first approximation, and is the first quantitative demonstration of

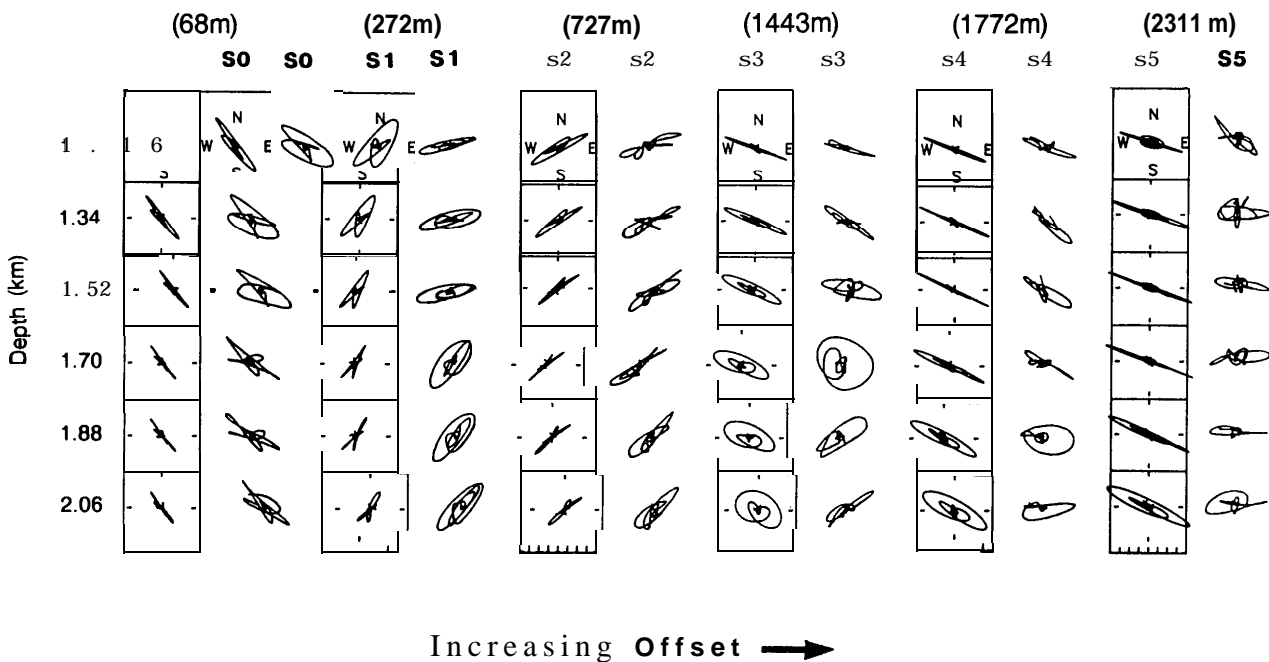


Figure 8. Observed shear-wave polarization diagrams (open columns) compared with synthetic shear-wave diagrams (boxed columns) for propagation through a model with cracks striking N30°W, from model parameters given in Table 4.

Table 4. Parameters of isotropic model containing distributions of parallel, vertical, water-saturated microcracks ($\rho = 1000 \text{ kg m}^{-3}$, $\lambda = 2.25 \times 10^9 \text{ Pa}$, $\mu = 0.0 \text{ Pa}$, and negligible aspect ratio, $AR = 0.0001$).

| Layer thickness (m) | ρ (kg/m ³) | V_p (m/s) | V_s (m/s) | Crack density | Crack strike (N°W) |
|---------------------|-----------------------------|-------------|-------------|---------------|--------------------|
| 800 | 2600 | 2800 | 1300 | 0.024 | 30 |
| 300 | 2600 | 4350 | 2350 | 0.024 | 30 |
| 700 | 2600 | 4350 | 2350 | 0.016 | 30 |
| halfspace | 2600 | 3600 | 1a00 | 0.016 | 30 |

EDA cracks in a sedimentary basin (Crampin & Bush 1986; Crampin et al. 1986). The synthetic patterns in Fig. 8 are the most recent results (Bush 1990).

6.5 Discussion of anomalous shear-wave motion

We suggest that the synthetic patterns match the observed patterns in Fig. 8 reasonably well except the following.

(1) The overall orientations of synthetic patterns for the three shallowest geophones in the S1 offset are oriented approximately 30° anti-clockwise from the observed patterns, although the orientations of the deeper patterns are well matched.

(2) The observed particle motion patterns for the S3 offset range from nearly linear polarization in an ESE direction at the shallower geophones, through elliptical motion, to nearly linear motion in a NE direction at the deeper geophones. Synthetic particle motions show a behaviour similar to the observed patterns at the shallow and intermediate depth geophones, but fail to model the patterns observed for deeper geophones.

(3) The observed motions for the S4 offset range from linear motion in the ESE direction for the shallowest geophone to flattened elliptical motion in the ENE direction at the deepest, whereas the synthetic patterns show approximately linear ESE motion at all depths.

(4) Observed particle motion patterns for the S5 offset show much scatter, even between geophones spaced 15 m apart (not shown), and it is likely that for such wide offsets (large angles of incidence) the shear waves are disturbed by irregularities in the interfaces (see discussion in Section 5).

The patterns in the other offsets are reasonably well matched, and only minor differences exist. Synthetic polarization diagrams in the SO offset are less elliptical than the observed motions, yet are a good match of the delays. Synthetic diagrams for the S2 offset have a smaller delay than the observed motions. Reducing the crack density above 1100 m and increasing it beneath 1100 m considerably improves the match for the S1 diagrams, yet the match at SO becomes worse (Bush 1990). These modelling results indicate that the observed split shear waves from S1 may have smaller delays than those from SO. These anomalous motions (misfits between observed and synthetic diagrams) in the S1, S3, and S4 offsets are investigated in this paper and constitute the basis for our final conclusions.

7 SOURCE AND RECEIVER EFFECTS

The polarization, amplitude, and phase of the emitted source-wavelet may change because of different vibrator baseplate couplings (Hardage 1985); ground-force output levels (Lerwill 1981; Edelmann 1982; Sallas 1984); and repositioning of the source with slightly different orientations. Bush (1990) shows, by means of synthetic seismograms, that the transmitted wave-motions are sensitive to the source orientation and phase but varying these parameters cannot explain the anomalous wave-motions observed on the S1, S3 and S4 offsets. We find no evidence to suggest poor coupling between the tool and borehole wall, which could affect the recorded signal. The main modal resonances of the three-component tool are well outside the frequency range of the shear waves to have affected the recorded signal (A. Green, personal communication).

Analysis of the repeated S4 offset suggests that polarization diagrams have slightly different orientations (approximately $\pm 4^\circ$) when the tools have different orientations in the well (Bush 1990). Such asymmetric tool response may arise from the different response of the horizontal components, parallel and perpendicular to the locking arm (Montmollin 1988). However, this asymmetry is minor compared with the errors of three-component tool reorientation, which is accurate from $\pm 6^\circ$ at best to $\pm 14^\circ$ at worst (Bush 1990). These errors (estimated from the variance of particle motion orientations between neighbouring geophone levels displaying similar patterns) limit the accuracy with which polarization diagrams can be measured. We conclude that the changes in overall particle motion orientations, down the S1, S3, and S4 offsets cannot be explained in terms of source or receiver effects and must be in response to a real subsurface geological condition.

8 ROCK-MATRIX PROPERTIES

We inverted the body-wave traveltimes for velocity and noted differences with the sonic velocities. To invert accurately for crack parameters a detailed knowledge of the rock-matrix properties is required. The anomalous inverted velocities indicate values (relatively high sonic velocities) possibly due to the effects of anisotropy. We studied synthetic seismograms for different background velocity structures, to ascertain the effects of the rock-matrix properties on the shear-wave motions.

8.1 VSP travelttime-velocity inversion

The compressional- and shear-wave traveltimes were inverted for velocity, for the different source offsets and azimuths, and a mean velocity profile calculated (Bush 1990). The VSP and sonic velocities indicate a similar velocity structure and are in agreement with other field observations (Stewart, Huddleston & Kan 1984). The sonic velocities are in general faster than the inverted velocities from the VSPs (Fig. 9). Note that the sonic logs were uncalibrated, as the physical meaning of calibrated sonic logs, when the velocity varies with direction, is not well understood. Anisotropy is likely to affect sonic and VSP velocities in different ways, because of their very different

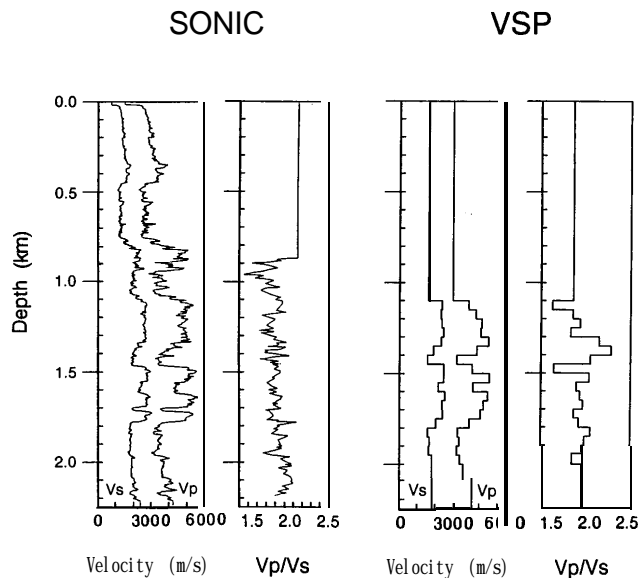


Figure 9. Comparison of sonic velocities and their ratio, V_p/V_s (sonic), with the inverted seismic velocities and their ratio, V_p/V_s (VSP). The seismic velocities are a weighted average of the velocities inverted from the traveltimes for each individual VSP. The average velocities are weighted according to the maximum travelt ime error (differences between observed and calculated traveltimes) of each VSP, so that VSP velocities with large errors have a small weighting and contribute little to the average model. The inverted velocity structure consists of a single layer above 1100 m with 50 m thick layers within the geophone range. The velocity above 1100 m represents the average velocity over this depth range, and below 2050 m the velocity is continued at the 2050 m value.

wavelengths. However, the main reason for the observed differences is believed to be that sonic logs sample only the rock immediately surrounding the borehole. This is likely to have been altered during the drilling process (Goetz, Dupal & Bowler 1979), so that its velocities could be significantly different from the *in situ* velocities sampled by the VSP.

The inversion procedure (Pujol, Burridge & Smithson 1985, 1986) assumes a horizontally layered isotropic medium and it is probable that the velocity errors, introduced by assuming isotropy, are comparable to the magnitude of the percentage of anisotropy. The P-wave and shear-wave velocities indicate a general increase in velocity with offset (Bush 1990). Since the layering in the Paris Basin is believed to be almost horizontal, this result could be interpreted as the horizontal velocities being faster than the vertical velocities, or over compensation in the modelling correction from apparent to true velocity.

The compressional- and shear-wave velocities, from wide-offset sources, are respectively 7 per cent and 14 per cent faster than the near-offset velocities for the top 1100 m (Bush 1990). However, the shear-wave velocities in the top 1100 m are 2.7 per cent slower in the S1 profile than those in the SO, despite the S1 source being at a wider offset. We would expect similar velocity variations to occur in orthorhombic media, arising from combinations of vertically aligned cracks and PTL anisotropy. The comparatively slow velocity, inverted from S1, could be due to shear waves travelling at incidence angles close to a point singularity.

Shear-wave propagation in orthorhombic media is examined below. However, the slower shear-wave velocity for the S1 profile could also indicate a different structure in the top 1100 m.

Using the inverted velocities, the shear-wave velocity in the upper section of the three-layered model was redefined as $V_s = 1.49 \text{ km s}^{-1}$, rather than 1.3 km s^{-1} , as in Table 4. The original approximate shear-wave velocity of 1.3 km s^{-1} was calculated from the compressional-wave log assuming a velocity ratio of 2.15. The revised shear-wave velocity of 1.49 km s^{-1} is calculated from the compressional-wave log and the seismic velocity ratio of 1.9 ± 0.2 observed in the top 1100 m.

8.2 Near-surface low-velocity layer

Delays between split shear waves are inversely proportional to the shear-wave velocities of the rock-matrix. Consequently, the differential time delays increase for propagation through cracked rock with a lower matrix velocity. A near-surface low-velocity layer (LVL) may delay traveltimes and, consequently, different LVL thicknesses at each source position can give rise to different observed delays between split shear waves. Compared with the SO profile, the data from S1 indicate a lower average velocity in the top 1100 m suggesting that a thicker LVL, or a lower velocity within the LVL, could be present beneath the S1 source position. However, to account for the considerably smaller differential shear-wave delays observed on S1 requires that an LVL is thinner at the S1 source location.

This difficulty suggests that the smaller anisotropies and the lower velocities at the S1 profile cannot be explained by the presence of crack anisotropy in a near-surface LVL. Furthermore, sonic logs at the borehole site (Fig. 9) do not indicate an LVL extending to a sufficient depth to increase the delays between split shear waves at the SO offset, so it appears that this condition is unlikely to exist.

8.3 Multilayered crack model

An accurate velocity structure is important not only to model the correct arrival times, but also to model the correct shear-wave polarizations and delays. Waves incident at an interface at angles greater than the critical angle become distorted by the effects of mode conversions and phase rotations (Douma & Helbig 1987; but see Liu & Crampin 1990). This may be important for the wide-incidence ray paths from the far-offset source locations S3, S4 and S5. We distinguish this multilayered model (20 layers) from finely layered models by the criterion that the seismic waves do not satisfy the long-wavelength conditions (seismic wavelengths substantially greater than the thickness of the individual layers), and thus the medium cannot be replaced by an equivalent set of elastic constants.

Synthetic seismograms in the multilayered cracked model show only minor modifications to the patterns in the polarization diagrams (Bush 1990), although the wide-offsets do have numerous reflected arrivals. This is most pronounced at shallowest geophones, and the widest offset S5, where ray paths have largest incidence.

9 CRACK PARAMETERS

In principle, the orientation, density, shape, and internal contents of the cracks, and the distribution of the crack populations, can be estimated from the synthetic seismic response to changes of crack properties.

9.1 Crack orientation

A change of 5° in crack orientation is sufficient to create noticeable changes in synthetic polarization diagrams, suggesting that we can resolve crack orientations with an accuracy of at least $\pm 5^\circ$ (Bush 1990). Since the VSP data are recorded between 1100 and 2060 m, we are unable to resolve any spatial variation of crack orientation above the top geophone. We find no evidence to suggest that cracks rotate in the depth range surveyed by the profiles. Modelling suggests that a homogeneous crack orientation $N30^\circ W \pm 5^\circ$ provides the best model.

9.2 Crack density between the surface and the top geophone

Since there are no observations recorded above 1100 m, we cannot determine whether the shear-wave delays at 1100 m are due to a homogeneous crack density above 1100 m, or a large concentration of cracks over a short depth-interval somewhere between the surface and 1100 m. The presence and alignment of cracks near the free surface is likely to be complicated (Crampin 1990b). If the observed anisotropy were due to a large density of fractures in the near-surface, any lateral variation of the thickness or fracture density of the weathered layer would result in different delays recorded on the individual VSPs. This could explain the small delays observed at the S1 offset, however, to support this idea, we would require further information about the near-surface geology. The S1 offset is better modelled with a smaller crack density ($CD = 0.010 \pm 0.002$) in the top 1100 m (Bush 1990).

Such a crack density causes a differential shear-wave delay of approximately 8 ms for propagation from the S1 offset to 1100 m. This compares with a 20 ms delay observed at the SO offset. We find that the differential shear-wave time delays observed in the SO offset are approximately double those observed from S1, and can be modelled by shear-wave propagation through a volume of rock in the top 1100 m with approximately double the crack density. Rock properties change with lithology, but since the strata is horizontally bedded we do not expect large lateral variations of lithology or other rock properties. We therefore suggest that, in the area of the borehole, the crack properties are unlikely to vary substantially laterally. Since the observed shear-wave motions are in response to the subsurface geology and large lateral variations of crack properties are unlikely, the different shear-wave delays appear to be due to the shear-wave propagation paths having different azimuths and incidences through the rockmass. Such large variations of delays over small angular directions are expected close to point singularities.

9.3 Crack density between the top and bottom geophones

Between 1500 and 1600 m, the observed polarization diagrams from the S1 offset rotate, suggesting an abrupt change in the behaviour of split shear waves between these depths. Using a spectral interference method for measuring the effects of anisotropy (MacBeth & Crampin 1991), measurements of differential shear-wave delays in the S1 offset from -7ms at 1100 m to -14ms at 2060 m, (C. D. MacBeth, personal communication) confirm an abrupt increase of delay around a level of 1600 m. These anomalously low delays confirm our previous results of synthetic modelling. For a homogeneous anisotropic rock the delay increases linearly with the path length, suggesting that an abrupt increase in delay could indicate an increase of anisotropy in the rock, particularly an increase of crack density.

In a layered anisotropic structure, the delay may also increase due to a change of incidence angle or a change of velocity. For the near-vertical ray paths from the near-offset sources, there is little change of incidence across interfaces, and it is unlikely that the changes in delay are due to the changes in incidence angles. Previous modelling with a multilayered structure indicates only small increases of delay associated with low-velocity layers. We therefore conclude that the increase in the observed delays is due to an increase in the anisotropy at, or above, this level. This is best modelled with synthetic seismograms for the SO offset propagating through a cracked model, with a large crack density of $CD = 0.12 \pm 0.04$ in the 1500 to 1600 m interval and a small crack density of $CD = 0.005$ for the rest of the model below 1100 m (Bush 1990). [Note that the formulations of Hudson (1980, 1981) become progressively less accurate for crack densities greater than $CD = 0.1$, but $CD = 0.12$ is only just outside the valid range and the values will be reasonably accurate.] Independent evidence of, possibly very small, cracks is not easy to obtain (Crampin 1987a), and apart from this seismic evidence there is no other support for the larger crack density between 1500 and 1600 m.

9.4 Crack aspect-ratio and pore-fluid properties

In the crack formulations of Hudson (1980, 1981), the crack-filling substance, which in sedimentary rocks is the pore-fluid, appears only in combination with the crack aspect-ratio. This means that it is impossible to determine the aspect-ratio unless the pore-fluid properties are known independently. Crampin & Atkinson (1985) suggest that cracks are probably fluid-filled at most depths in the Earth's crust (where the fluid is usually liquid water, possibly heavily mineralized, but may also be a gas-water or oil-water mixture in hydrocarbon reservoirs). The main exception to this is likely to be very close to the surface, where cracks may be partially or wholly unsaturated (Crampin, McGonigle & Bamford 1980). If we assume that the fluid properties do not change (which in reality may not be the case during enhanced oil recovery), the behaviour of shear-wave splitting carries information about the aspect-ratio.

Douma (1988) compares the crack formulations of Nishizawa (1982) with those of Hudson (1980, 1981), and finds that the two procedures give similar results for crack aspect ratios up to $AR = 0.3$ (for crack density $CD = 0.05$). We have used both formulations in our investigations. Ray paths for the wide-offset profiles cover a range of incidences from approximately 40° to 70° , and would be expected to sample incidence angles close to line singularities [where the shear-wave phase-velocity sheets intersect (see Crampin & Yedlin 1981)]. Since line singularities move towards the symmetry axis as the aspect ratio increases (Crampin 1991a) and pore-fluid velocities increase, shear waves recorded in the S3 offset are likely to be affected by such changes of crack properties. Polarization diagrams of synthetic shear waves propagating through models of water-saturated cracks indicate that the shear-wave motions from S3 are affected by changing the crack aspect-ratio (Bush 1990). An aspect ratio of 0.3 improves the modelling of the S3 offset, but the change is not sufficient to match the observations closely.

9.5 Crack distributions

Modelling EDA cracks as a single homogeneous system of parallel aligned cracks may be over idealized, since cracks probably have a distribution of alignments about a predominant direction. Up to now in this paper, we have modelled only distributions of parallel aligned cracks, where the crack orientations form a single distribution with no variance. Hudson (1986) extends his (1980, 1981) crack formulations to the case where the cracks consist of two or more parallel sets aligned in different directions. Using these formulations, we have modelled two types of crack distribution:

- (1) cracks striking with an azimuthal orientation $N30^\circ W$, but with a range of dips from the horizontal; and
- (2) cracks aligned vertically, but with a range of strikes.

In order to maintain a constant delay for vertically propagating shear waves, crack densities must be increased as the range of crack strikes, or dips, widens. Polarization diagrams for synthetic shear-wave propagation, through populations of cracks striking $N30^\circ W$ and with a large distribution of dips, indicate that the patterns of polarization for the bottom geophones of the S3 offset rotate with depth in a manner similar to the observations, whereas diagrams for the other offsets show little change (Bush 1990). In contrast, polarization diagrams for synthetic shear waves propagating through populations of vertically aligned cracks show little change in the patterns of polarization as the angular distribution of strikes increases (Bush 1990).

10 COMBINATIONS OF PTL AND EDA ANISOTROPY

We have previously demonstrated that the presence of fine-layering and lithologic anisotropy (PTL anisotropy) at the well site cannot alone account for the observed shear-wave splitting at the near-offset profiles. However, the observed shear waves for the zero-offset profile can be modelled with the azimuthal anisotropy of vertically aligned EDA cracks. Combinations of PTL anisotropy and EDA crack anisotropy seem indicated. Since fine-layering and

lithologic anisotropy have TI with a vertical axis of symmetry (azimuthal isotropy), and EDA crack anisotropy has TI with a horizontal axis, the combination leads to orthorhombic anisotropic symmetry.

The shear-wave phase-velocity sheets in a solid with TI symmetry meet in a circle about the symmetry axis and can be thought of as intersecting in a line singularity (Crampin & Kirkwood 1981; also see fig. 1 of Crampin 1991b, this issue). Combining parallel cracks orthogonal to the azimuthal isotropy of PTL anisotropy yields a rock with orthorhombic symmetry in the long-wavelength limit (Crampin 1978). The line singularity pulls apart and the two shear-wave phase-velocity sheets touch in a number of discrete point singularities along the pull-apart line singularities (fig. 2 of Crampin 1991b). A point singularity is a place where the two surfaces are continuous with each other through the vertices of cone-shaped projections from the surfaces (Crampin & Yedlin 1981). The behaviour of shear-wave ray paths, propagating at the group velocity, near point singularities may be complicated (Crampin 1991b; Wild & Crampin 1991). For shear-wave ray paths propagating in a plane, which cuts the slowness surfaces near a singularity, the velocities of the two shear waves approach each other in a ring pinch (Crampin & Yedlin 1981) and at the pinch exchange polarizations. This means that the polarization of the leading split shear wave, $qS1$, may abruptly swing through 90° for small changes in direction near point singularities or pull-apart line singularities.

Figure 10 shows a comparison of synthetic and observed shear-wave polarization diagrams for a model containing combinations of PTL anisotropy and EDA crack anisotropy. The crack distributions have the same parameters as before (Table 4) but are combined with 4 per cent PTL anisotropy, using Hudson's (1986, 1991) formulations. The difference in size of the patterns at the S1 offset is due to a different normalization for the two columns, and the synthetic and observed polarization diagrams are well matched at all offsets, except for the S5 offset.

Referring to the previous anomalies listed in Section 6.5:

- (1) In the S1 offset, the top and bottom synthetic polarization diagrams now match the observations, although the transition from one orientation to the other is not as abrupt as in the observed diagrams.
- (2) In the S3 offset, the transition from linear motion at one orientation, through elliptical motion, to linear motion at another orientation is well matched.
- (3) Similarly, in the S4 offset, the transition from linear motion to elliptical motion is well matched.
- (4) We consider that the irregular behaviour in the S5 offset is caused by minor irregularities at the interfaces, and cannot be matched by the homogeneous models we are using here.

These results indicate that the observations from the S3 offset can be modelled with ray paths close to the transition zone where the previous line singularity has pulled apart and the shear-wave phase-velocity surfaces now approach yet do not intersect (Bush 1990; Bush & Crampin 1989; Crampin 1991b). The behaviour of the oriented patterns in the polarization diagrams is critically dependent on the ratio of the fine-layer or lithologic anisotropy (4 per cent) to crack

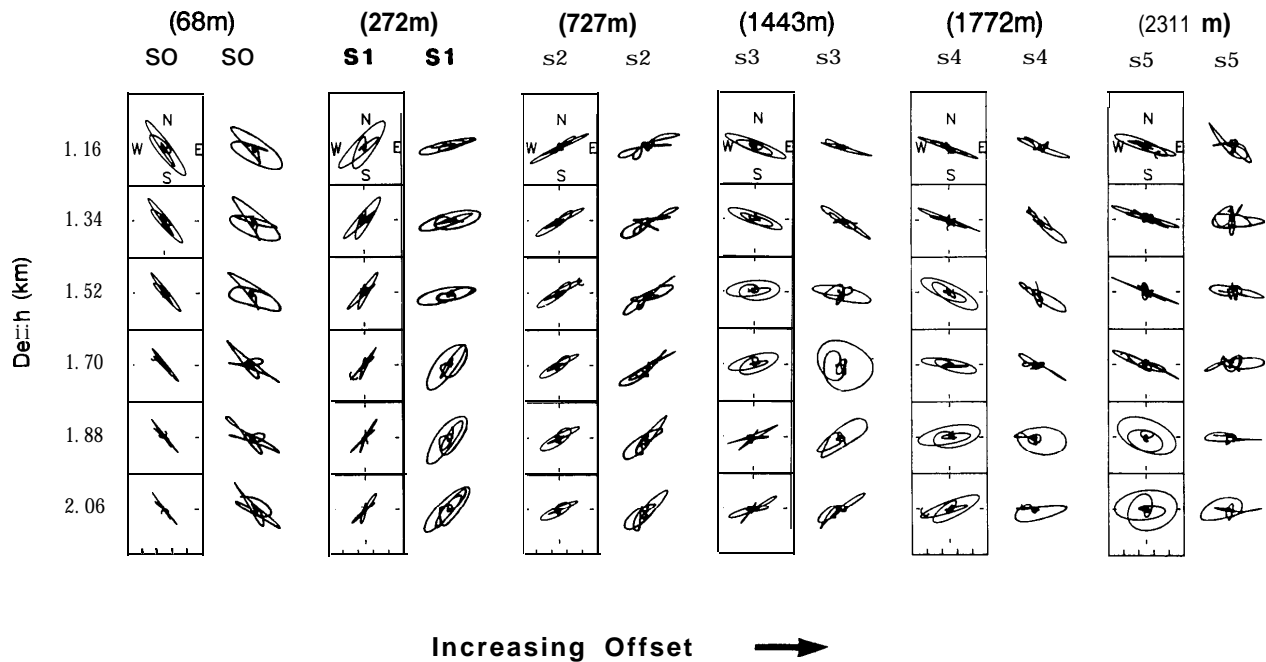


Figure 10. Comparison of observed shear-wave polarization diagrams (open columns) with synthetic diagrams (boxed columns) for propagation through combinations of vertical fluid-filled EDA cracks and 4 per cent PTL anisotropy. The other model parameters are listed in Table 4, except that the shear-wave velocity in top layer has been changed to 1490 m s^{-1} .

anisotropy (1-2 per cent) (Bush & Crampin 1989; Wild & Crampin 1991). We now briefly discuss the principles that have guided us in choosing appropriate combinations. More complete discussions can be found in Bush (1990).

10.1 Magnitude of PTL anisotropy

Assuming that the crack distributions are vertically aligned and that the fine-layering (leading to PTL anisotropy) is horizontally stratified (vertical symmetry axis), the observed delays at strictly vertical incidence can be attributed almost entirely to EDA cracks. Consequently, the observed shear-wave delays, from the SO offset, may be attributed to EDA cracks alone. The crack parameters are therefore constrained within limits, obtained from the SO offset observations, and allow ranges of PTL anisotropy to be examined (3 to 5 per cent). The main effect of increasing the PTL anisotropy is to increase the shear-wave delays for wide-incidence ray paths. However, increasing the fine-layer anisotropy also causes the point singularities to move position (Wild & Crampin 1991).

10.2 Multilayered model with combinations of EDA crack and PTL anisotropy

Interpreting the observations in terms of point singularities requires some understanding of the behaviour of the shear waves through all the layers of the model. The different shear-wave polarizations as a shear wave is refracted, from one layer to another, may give rise to anomalous motion (Liu & Crampin 1990), particularly in directions close to singularities where the shear-wave polarizations and delays change rapidly. Since shear waves for the S1 offset propagate along nearly vertical ray paths, the effects of

refraction at a horizontal interface are less than for rays with wide offsets. Consequently, there is little difference in the synthetic seismograms for the S1 offset as a result of including more layers, although there may be significant effects at wider offsets.

10.3 Crack aspect-ratio and pore-fluid properties in PTL anisotropy

We previously demonstrated that increasing the crack aspect-ratio or changing the pore-fluid properties moves the line singularity (where the two phase-velocity sheets intersect) to wider incidence angles. Similarly, with a combination of EDA crack and PTL anisotropy, an increase of the crack aspect-ratio causes the point-singularities to move systematically (Wild & Crampin 1991). Fig. 11 shows approximate positions of point singularities in the 700 m thick layer (Table 4) for a variety of crack aspect ratios. The solid bar marks the approximate position of the ray paths sampled by the S3 offset. The bar crosses the transition zone of the pull-apart line singularity, and shows why the observed polarizations swing through nearly 60° down the geophone column.

Increasing the crack aspect-ratio causes polarization diagrams for the S4 and S5 offsets to rotate in a manner similar to S3. Numerous calculations (Bush 1990) demonstrate that the wide-offset profiles are sensitive to the crack aspect-ratio. The wide-offset profiles are well matched to the synthetic motions for a model consisting of combinations of 4 per cent PTL anisotropy and vertically aligned EDA cracks with aspect-ratios in the range $0.05 \leq AR \leq 0.1$ with water as pore-fluid. With larger crack aspect ratios, the S3 offset can possibly be modelled with a smaller PTL anisotropy. Thus, given the uncertainty in the

4% PTL, CD = 0.016 aligned N30°W

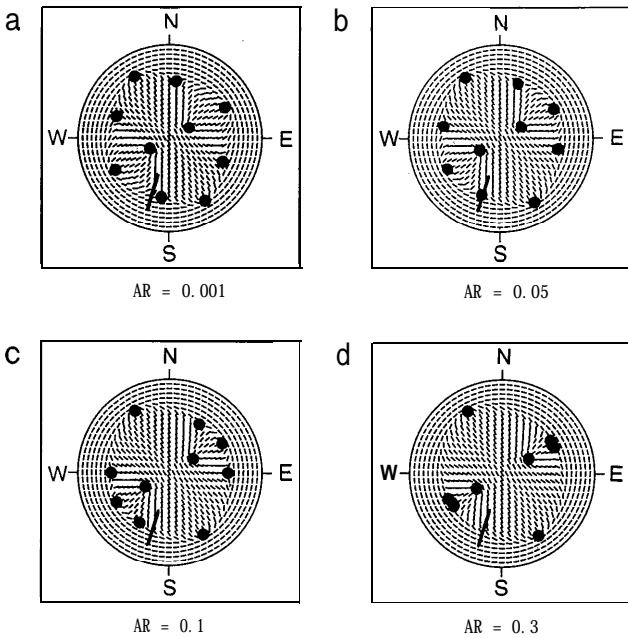


Figure 11. Equal-area projections of $qS1$ polarizations in a hemisphere of directions for a combination of PTL and EDA anisotropy, modelling the 700m thick layer in Table 4. The rock matrix has velocities: $V_p = 4.35 \text{ km s}^{-1}$ and $V_s = 2.35 \text{ km s}^{-1}$. There is 4 per cent differential shear-wave PTL anisotropy, and the cracks have crack density $CD = 0.016$ aligned N30°W, and have a range of aspect-ratios: (a) $AR = 0.001$; (b) $AR = 0.05$; (c) $AR = 0.1$; and (d) $AR = 0.3$. The black dots indicate the position of singularities on the phase-velocity sheets, and the solid bar indicates the range of incidence angles sampled by the S3 offset.

PTL anisotropy (4 ± 1 per cent), the range of possible aspect ratios extends to $0.00011 \text{ } AR \leq 0.3$.

10.4 Dipping cracks imbedded in PTL anisotropy

We constructed a model with cracks inclined 15° from the vertical (dipping 75° to the SW) throughout the whole structure. In this model, synthetic polarization diagrams for the near-offsets S1 and S2 both match well the observed diagrams. This is largely because ray paths for the S1 offset sample directions close to a point singularity and consequently the delays are relatively small, so that synthetic seismograms for S1 display the characteristic change of particle motion with geophone level.

In contrast, the ray paths for the SO offset in this model sample directions away from this singularity and experience a larger delay. This is the sole model we found which matches the observed and synthetic seismograms for both SO and S1 offset, and confirms that the 50 per cent difference in the observed delays at the two near-offset profiles can be modelled as ray paths close to a singularity. However, this model cannot match seismograms for the wide-offset profiles and, in particular, the rotation of polarization diagrams on the S3 offset, indicating that this is a poor model for the wide offset ray paths, and this model is rejected.

11 DISCUSSION

We have attempted to invert these multi-offset observations for the rock properties surrounding the borehole. We summarize our results in Table 5. We have found that the observations can only be modelled by wave propagation through combinations of EDA crack and PTL anisotropy. The EDA crack distribution has mean values of differential shear-wave anisotropy of 2.7 ± 0.2 per cent from 0 to 1100 m and 1.8 ± 0.4 per cent from 1100 to 2060 m, whereas the PTL anisotropy has mean values of anisotropy of 4 ± 1 per cent. Combinations of EDA crack and PTL anisotropies with orthogonal symmetry axes, yield an orthorhombic symmetry system in which shear-wave phase-velocity sheets are analytically continuous only at discrete point singularities. The relative positions of the point singularities are affected by the particular combinations of EDA crack and PTL anisotropy, and consequently the positions of the singularities tightly constrain the model parameters (Bush 1990).

In assessing the significance of the observations it is essential to consider the effects of possible errors. We have inverted the data by matching synthetic and observed shear-wave motions. This procedure depends on the ability to recognize subtle differences in waveform, and being subjective is open to errors. Automated techniques for

Table 5. Estimated values and uncertainties of parameters defining the optimum model for the Paris Basin VSPs. The crack densities are given for two models: (1) a homogeneous distribution of cracks below 1100 m (polarization diagrams in Fig. 10); and (2) a more detailed distribution (polarization diagrams very similar to Fig. 10). These uncertainties are the range of values with which the parameters have been resolved from modelling and do not include the uncertainties in the rock-matrix velocities and tool orientation. Note that the crack parameters change for the different background models.

| MODEL PARAMETERS | VALUE AND UNCERTAINTY |
|------------------------|---|
| Crack density (1) | |
| 0 - 1100m | 0.024 ± 0.004 |
| below 1100m | 0.016 ± 0.005 |
| Crack density (2) | |
| 0 - 1100m | 0.024 ± 0.004 |
| 1100m - 1500m | 0.005 ± 0.001 |
| 1500m - 1600m | 0.12 ± 0.04 |
| below 1600m | 0.005 ± 0.001 |
| Crack strike | N30°W \pm 5° |
| Crack dip | 90° |
| Crack aspect-ratio | 0.0001 to 0.3 |
| Pore fluid | Unknown (water assumed) |
| Crack distribution | Unknown (assumed uniform) |
| PTL-anisotropy | Differential shear-wave anisotropy of $4\% \pm 1\%$ |
| Rock matrix properties | |
| 0 - 800m | $V_p = 2.8\text{km/s}; V_s = 1.49\text{km/s}$ |
| 800m - 1800m | $V_p = 4.35\text{km/s}; V_s = 2.35\text{km/s}$ |
| below 1800m | $V_p = 3.6\text{km/s}; V_s = 1.8\text{km/s}$ |

extracting shear-wave polarizations and delays are expected to improve the sensitivity to changes of shear-wave splitting (MacBeth 1991a, b). The uncertainties associated with each parameter in Table 5 represent the range of values over which the parameter can vary before the seismic response displayed in polarization diagrams changes significantly. In general, the resolution of crack properties depends upon: the thickness of the zone of interest; the background rock-matrix; and the source and receiver parameters. The largest source of error in VSP data sets is probably in the determination of the orientation of the three-component geophone tool. These inaccuracies limit our ability to resolve directional quantities and hence wave polarizations. The values for the parameters in Table 5 do not include the instrumental errors and the uncertainty in the background rock-matrix velocity. In other data sets with better signal-to-noise ratios, better tool orientations, and several source azimuths, the accuracy may be improved.

It has been impossible to establish the near-surface properties without observations about 1100 m; nevertheless shear-wave splitting is present from this upper section and can be attributed to a distribution of aligned cracks with a mean crack density of 0.024. Though it is unlikely that a heavily cracked near-surface layer can account for the differences in shear-wave delays between the SO and S1 offsets, we cannot exclude this without further geophysical information. In the depth range surveyed by the VSPs below 1100 m, a more detailed structure has been resolved. The section between 1100 and 2060 m has a mean crack density of 0.016, however, a zone of increased anisotropy has been identified between approximately 1500 and 1600 m. In the depth range surveyed by the VSPs, the lower sections can be modelled by a relatively large crack density of 0.12 in a 100 m thick layer from 1500 to 1600 m, and a weak crack density of 0.005 in the remaining section beneath 1100 m. An increase in crack density could be interpreted as the rock containing more cracks and having an increased permeability and possibly porosity. However, it could also be interpreted as the overall crack population, and hence porosity, remaining constant, but with a greater proportion of the crack population being aligned parallel. If the cracks were interconnected this would increase the permeability (or fluid-flow) parallel to the cracks. We have not resolved the crack distribution and therefore cannot distinguish between these two quite different interpretations.

Larger (finite) aspect-ratio EDA cracks combined with PTL anisotropy, have a significant effect on PD patterns recorded from wide-offset VSPs. The effects of the pore-fluid and crack aspect-ratio on the split shear waves are inseparable. If nothing is known about either, then no unique value can be determined. Since cracks at depth are most likely to be fluid filled (without the pore-pressure, cracks would tend to close), we have assumed the cracks to be water-filled. With this assumption we are able to resolve a range of aspect-ratios from 0.0001 to 0.3. Changes of aspect-ratio could lead to a change of porosity.

We find that a homogeneous distribution of cracks aligned N30°W \pm 5° provides the best model, but there are some indications that the crack dip may not necessarily be vertical. We have shown that a point singularity at near-vertical incidence is most likely responsible for the 50

per cent difference in the shear-wave delays observed between the SO and S1 offsets. Dipping the cracks 75° from the horizontal produces an excellent match for the near-offset, but does not succeed in matching the wide-offset profiles. Similarly models which match well the wide-offset profiles do not succeed in matching the near-offsets.

12 CONCLUSIONS

The rock surrounding the borehole site has, at least, an orthorhombic anisotropic symmetry persisting to several seismic wavelengths away from the borehole. The most likely cause of such anisotropic symmetry is the combination of EDA crack and PTL anisotropies. Vertically aligned EDA cracks imbedded in horizontally stratified PTL anisotropy yields orthorhombic symmetry. A singularity at near vertical incidence appears to be responsible for the considerably different delays observed between the two near-offset profiles SO and S1. Similarly, a transition zone, close to a singularity, where there are rapid changes of shear-wave polarization and delay is responsible for the anomalous motions observed in the wide-offset S3.

Singularities are expected to occur for propagation in most sedimentary rocks (Wild & Crampin 1991). Consequently, the interpretation and modelling of shear waves in sedimentary basins should take into account the possible effect of singularities on the behaviour of shear-wave polarizations and delays within the rockmass. These effects include the variation of shear-wave polarizations for near-vertical propagation in a common depth gather, and abrupt changes of delays for small changes of propagation direction. Shear-wave singularities may occur at almost any incidence and azimuth, and their relative positions on the phase-velocity sheets tightly constrain the modelling of EDA crack and PTL anisotropy (Wild & Crampin 1991).

Matching synthetic to observed polarization diagrams requires an almost identical agreement in amplitude and phase between two orthogonal seismic components. Substantial inaccuracies or errors in any one of these developments would have prevented any match of synthetic to observed polarization diagrams. The excellent match of synthetic to observed polarization diagrams in Fig. 10 is confirmation that the various techniques used in this analysis are appropriate for sedimentary basins and indicate the presence of combinations of PTL and EDA anisotropy in sedimentary basins. We suggest the modelling provides confirmation of the EDA crack hypothesis (Crampin *et al.* 1984; Crampin 1987 a, b); the crack formulations of Hudson (1980, 1981, 1986); the modelling procedures of Taylor (1987, 1990).

We have also demonstrated the sensitivity of shear waves to crack parameters. This suggests that shear-wave VSPs may have applications to monitoring the progress of enhanced oil recovery operations. Changes of pore fluid properties will cause variations in the behaviour of shear-wave splitting, which can be monitored with appropriate shear-wave experiments.

ACKNOWLEDGMENTS

We wish to thank the French VSP Consortium [Institut Français du P&role, Compagnie Générale de Géophysique

(CGG), TOTAL Compagnie Française des P&roles, Elf Aquitaine, Gaz de France] for the VSP data. The VSP geophone sonde was the CGG 'Geolock H' tool. We also thank Applied Geophysical Software Inc. and Macro Ltd for approval to use the ANISEIS synthetic seismogram package. The study was performed while the first author was at the University of Edinburgh. This work was supported by the Natural Environment Research Council and the French VSP Consortium, and is published with the approval of the French VSP Consortium and the Director of the British Geological Survey (NERC).

REFERENCES

- Backus, G. E., 1962. Long-wave elastic anisotropy produced by horizontal layering, *J. geophys. Res.*, **67**, 4427-4440.
- Booth, D. C. & Crampin, S., 1983. The anisotropic reflectivity technique: theory, *Geophys. J. R. astr. Soc.*, **72**, 755-766.
- Booth, D. C. & Crampin, S., 1985. Shear-wave polarizations on a curved wavefront at an isotropic free-surface, *Geophys. J. R. astr. Soc.*, **83**, 31-45.
- Bush, I., 1990. Modelling shear-wave anisotropy in the Paris Basin, *PhD dissertation*, University of Edinburgh.
- Bush, I. & Crampin, S., 1987. Observations of EDA and PTL anisotropy in shear-wave VSPs, *57th Ann. Znt. SEG Meeting, Dallas, Expanded Abstracts*, pp. 646-649.
- Bush, I. & Crampin, S., 1989. The Paris Basin VSP: a classic case history demonstrating combinations of EDA- and PTL-anisotropy for the first time, *SEG Research Workshop, Recording and processing vector wave field data, Snowbird, Expanded Abstracts*, p. 69.
- Crampin, S., 1978. Seismic wave propagation through a cracked solid: polarisation as a possible dilatancy diagnostic, *Geophys. J. R. astr. Soc.*, **53**, 467-497.
- Crampin, S., 1981. A review of wave motion in anisotropic and cracked elastic-media, *Wave Motion*, **3**, 343-391.
- Crampin, S., 1984. Effective anisotropic elastic constants for wave propagation through cracked solids, *Geophys. J. R. astr. Soc.*, **76**, 135-145.
- Crampin, S., 1985a. Evaluation of anisotropy by shear-wave splitting, *Geophysics*, **50**, 141-152.
- Crampin, S., 1985b. Evidence for aligned cracks in the earth's crust, *First Break*, **3**, 3, 12-15.
- Crampin, S., 1987a. The geological and industrial implications of extensive-dilatancy anisotropy, *Nature*, **328**, 491-496.
- Crampin, S., 1987b. Crack porosity and alignment in shear-wave VSPs, in *Shear-Wave Exploration, Geophysical Developments, SEG Special Publication*, vol. 1, pp. 227-251, eds Danbom, S. H. & Domenico, S. N., Tulsa, OK.
- Crampin, S., 1989. Suggestions for a consistent terminology for seismic anisotropy, *Geophys. Prosp.*, **37**, 753-770.
- Crampin, S., 1990a. The potential of shear-wave VSPs for monitoring recovery: a letter to management, *The Leading Edge*, **9**, 3, 50-52.
- Crampin, S., 1990b. Alignment of near-surface inclusions and appropriate crack geometries for geothermal hot-dry-rock experiments, *Geophys. Prosp.*, **38**, 621-631.
- Crampin, S., 1991a. Wave propagation through fluid-filled inclusions of various shapes: interpretation of extensive-dilatancy anisotropy, *Geophys. J. Znt.*, **104**, 611-623.
- Crampin, S., 1991b. Effects of point singularities on shear-wave propagation in sedimentary basins, *Geophys. J. Znt.*, this issue.
- Crampin, S. & Kirkwood, S., 1981. Velocity variations in systems of anisotropic symmetry, *J. Geophys.*, **49**, 35-42.
- Crampin, S. & Yedlin, M., 1981. Shear-wave singularities of wave propagation in anisotropic media, *J. Geophys.*, **49**, 43-46.
- Crampin, S. & Atkinson, B. K., 1985. Microcracks in the Earth's crust, *First Break*, **3**, 3, 16-20.
- Crampin, S. & Bush, I., 1986. Shear-waves revealed: extensive-dilatancy anisotropy confirmed, *56th Ann. Znt. SEG Meeting, Houston, Expanded Abstracts*, pp. 481-484.
- Crampin, S., McGonigle, R. & Bamford, D., 1980. Estimating crack parameters from observations of P-wave velocity anisotropy, *Geophys. J. R. astr. Soc.*, **45**, 345-360.
- Crampin, S., Stephen, R. A. & McGonigle, R., 1982. The polarization of P-waves in anisotropic media, *Geophys. J. R. astr. Soc.*, **68**, 477-485.
- Crampin, S., Evans, J. R. & Atkinson, B. K., 1984. Earthquake prediction: a new physical basis, *Geophys. J. R. astr. Soc.*, **76**, 147-156.
- Crampin, S., Bush, I., Naville, C. & Taylor, D. B., 1986. Estimating the internal structure of reservoirs with shear-wave VSPs, *The Leading Edge*, **5**, 11, 35-39.
- Douma, J., 1988. The effect of the aspect ratio on crack-induced anisotropy, *Geophys. Prosp.*, **36**, 614-632.
- Douma, J. & Helbig, K., 1987. What can the polarisation of shear waves tell us?, *First Break*, **5**, 3, 95-104.
- Edelmann, H. A. K., 1982. A contribution to the investigation of amplitude characteristics of vibrator signals, *Geophys. Prosp.*, **30**, 774-785.
- Froidevaux, C., Paquin, C. & Souriau, M., 1980. Tectonic stresses in France: in situ measurements with a flat jack, *J. geophys. Res.*, **85**, 6342-6346.
- Goetz, J. F., Dupal, L. & Bowler, J., 1979. An investigation into the discrepancies between sonic log and seismic check shot velocities, *Austral. Petr. expl. Ass. J.*, **19**, 131-141.
- Hardage, B. A., 1985. Vertical seismic profiling. Part A: Principles, in *Handbook of Geophysical Exploration, Section 1, Seismic Exploration*, vol. 14a, eds Helbig, K. & Trietel, S., Geophysical Press, London.
- Hudson, J. A., 1980. Overall properties of a cracked solid, *Math. Proc. Camb. Phil. Soc.*, **88**, 371-384.
- Hudson, J. A., 1981. Wave speeds and attenuation of elastic waves in material containing cracks, *Geophys. J. R. astr. Soc.*, **64**, 133-150.
- Hudson, J. A., 1986. A higher order approximation to the wave propagation constants for a cracked solid, *Geophys. J. R. astr. Soc.*, **87**, 265-274.
- Hudson, J. A., 1991. Crack distributions which account for a given anisotropy, *Geophys. J. Znt.*, **104**, 517-521.
- Kaarsberg, E. A., 1968. Elasticity studies of isotropic and anisotropic rock samples, *Trans. Soc. Min. Eng.*, **241**, 470-475.
- Lerwill, W. E., 1981. The amplitude and phase response of a seismic vibrator, *Geophys. Prosp.*, **29**, 503-528.
- Liu, E. & Crampin, S., 1990. Effects of the internal shear wave window: comparison with anisotropy induced splitting, *J. geophys. Res.*, **95**, 11275-11281.
- MacBeth, C. D., 1991a. Inverting shear-wave polarizations for anisotropy using three-component offset VSPs: synthetic seismograms, *Geophys. J. Znt.*, this issue.
- MacBeth, C. D., 1991b. Inversion for subsurface anisotropy using estimates of shear-wave splitting, *Geophys. J. Znt.*, this issue.
- MacBeth, C. & Crampin, S., 1991. Examination of a spectral method for measuring the effects of anisotropy, *Geophys. Prosp.*, **39**, 667-689.
- Montmollin, V., 1988. Shaker tests on downhole seismic tools, *Geophysics*, **53**, 1160-1168.
- Naville, C., 1986. Detection of anisotropy using shear-wave splitting in VSP surveys: requirements and applications, *56th Ann. Znt. SEG Meeting, Houston, Expanded Abstracts*, pp. 391-394.
- Nishizawa, O., 1982. Seismic velocity anisotropy in a medium containing oriented cracks-transversely isotropic case, *J. Phys. Earth*, **30**, 331-347.

- Nur, A., 1989. Four-dimensional seismology and (true) direct detection of hydrocarbons: the petrophysical basis, **The Leading Edge**, **8**, **9**, 30-36.
- Pages, L., 1987. Exploration of the Paris Basin, in **Petroleum Geology of Northwest Europe**, pp. 87-93, eds Brooks, J. & Glennie, K. W., Graham & Trotman.
- Postma, G. W., 1955. Wave propagation in a stratified medium, **Geophysics**, **20**, 780-806.
- Pujol, J., Burridge, R. & Smithson, S. B., 1985. Velocity determination from offset vertical seismic profiling data, **J. geophys. Res.**, **90**, 1871-1880.
- Pujol, J., Burridge, R. & Smithson, S. B., 1986. Velocity determination from offset vertical seismic profiling data: Tests of the method, **J. geophys. Res.**, **91**, 701-708.
- Sallas, J. J., 1984. Seismic vibrator control and the downgoing P-wave, **Geophysics**, **49**, 732-740.
- Stewart, R. R., Huddleston, P. D. & Kan, T. L., 1984. Seismic versus sonic velocities: A vertical seismic profiling study, **Geophysics**, **49**, 1153-1168.
- Taylor, D. B., 1987. Double contour integration for transmissions from point sources through anisotropic layers as used in ROCPAC software, **Geophys. J. R. astr. Soc.**, **91**, 373-381.
- Taylor, D. B., 1990. **ANZSEZS Manual: Version 4.5**, Applied Geophysical Software Inc., Houston.
- Wild, P. & Crampin, S., 1991. The range of effects of azimuthal isotropy and EDA anisotropy in sedimentary basins, **Geophys. J. Znt.**, this issue.
- Yardley, G. & Crampin, S., 1991. Extensive-dilatancy anisotropy: relative information in VSPs and reflection surveys, **Geophys. Prosp.**, **39**, 337-355.

